

Force control of wire driving lower limb rehabilitation robot

Yupeng Zou^{a,*}, Huizi Ma^b, Zhiyuan Han^a, Yang Song^a and Kai Liu^a

^a*College of Mechanical and Electronic Engineering, China University of Petroleum, Qingdao 266580, Shandong, China*

^b*College of Mathematics and Systems Science, Shandong University of Science and Technology, Qingdao 266590, Shandong, China*

Abstract.

BACKGROUND: To solve the technical problems associated with the research on lower limb rehabilitation robot in terms of configuration design, human-machine compatibility, lightweight, and multimodel rehabilitation.

OBJECTIVE: This study introduced a parallel wire driving lower limb rehabilitation robot. The robot featured modular design, reconfiguration, multimodel, and good human-machine compatibility.

METHODS: The dynamics model of the wire driving module (WDM) was built based on which a multiple feedback loop controller (including a forward controller and a surplus force compensator) was designed.

RESULTS: The experimental results showed that the WDM could load force accurately and reliably during the loading procedure.

CONCLUSIONS: The machinery and control system of the WDM met the design request.

Keywords: Parallel wire driving robot, dynamics modeling, force control, lower limb rehabilitation

1. Introduction

In terms of the configuration of the robot, the lower limb rehabilitation robots can be divided into the exoskeleton-type and the footpad-type rehabilitation robots [1]. The exoskeleton-type rehabilitation robot drives the coordinated swinging of the legs of the patients, thereby assisting the patients to complete the rehabilitation exercise using the exoskeleton. Different gait training patterns can be realized by changing the movement patterns or the control strategies of the exoskeleton. The most typical exoskeleton-type product is Lokomat [2]. When patients can do some moderate active exercises, the exoskeleton becomes an assistance system, such as the Hybrid Assistive Limb of Tsukuba University and the ReWalk of Argo Medical Technologies [3,4]. The footpad-type rehabilitation robot, using pedals to drive the patient's feet, can simulate the natural walking motion of the feet. These kinds of robots can achieve different forms of gait training through controlling the pedals' attitude and motion. Stefan Hesse, who has been working on the footpad-type rehabilitation robot, has developed the production prototype G-EO System after the prototypes Gait Trainer and Haptic Walker [5]. Through optimization and improving the ordinary elliptical trainer, the research groups from the University of Nebraska-Lincoln and

*Corresponding author: Yupeng Zou, College of Mechanical and Electronic Engineering, China University of Petroleum, Qingdao 266580, Shandong, China. Tel.: +86 152 6622 0996; E-mail: zouyupeng@upc.edu.cn.

Madonna Rehabilitation Hospital developed an Intelligently Controlled Assistive Rehabilitation Elliptical trainer [6].

Presently, the research on the lower limb rehabilitation robots is associated with the following problems: (1) The existing exoskeleton-type rehabilitation robots have some disadvantages such as low stiffness, low precision, large inertia, and poor real-time capability. (2) It is difficult to implement single-joint training by using the footpad-type rehabilitation robot. (3) The DOF of the existing lower limb rehabilitation robot is limited, leading to movement deviation between the human body and the robot. The design of the robot needs to address problems pertaining to human-machine compatibility. (4) The drive system of the robot is required to work against the gravity of the mechanical body and the patient, resulting in high energy consumption and complex structure. It is necessary to carry out the lightweight design to improve the working efficiency. (5) The lower limbs are required to perform complex force/pose training in different rehabilitation phases. Most of the existing robots can realize pose control, but few robots can realize the complex force control.

In the wire driving mechanism, the wire replaces the rigid element as the transmission component. The wire driving mechanism has high load/weight ratio, high velocity/accuracy ratio, large working space, and adjustable stiffness. The wire driving robot has unique comprehensive advantages compared with traditional serial robots and parallel robots [7]. The application of wire driving mechanism in rehabilitation represents bright prospects because of the good flexibility. Some typical robots are available, such as MariBot, CAREX, C-ALEX, ROPES, PACER, and String Man [8–15].

In this study, a parallel wire driving robot (PWDR) was used to realize the rehabilitation of lower limbs, featuring modular design, reconfiguration, multimodel, and good human-machine compatibility. Figure 1 illustrates the structural scheme of the wire driving lower limb rehabilitation robot. The whole rehabilitation system was built on a treadmill. Four wire driving module (WDM) made up a planar PWDR. The robot could realize comprehensive rehabilitations, including passive rehabilitation, assistive rehabilitation, and initiative rehabilitation, by controlling the pose and force of the shank. The body-weight support unit was used to control the force that is applied on the lower limbs. The buffer springs were adopted to limit the motion of the pelvis of the subject. The pelvis of the subject could move freely within limits.

In the passive training process, the WDM took the initiative to drive the shank in accordance with the natural motion. The WDM was a position servo system. The gravity of the lower limb and the joint resistances were the external disturbances that had some effect on the position servo system. The WDM could achieve high position accuracy easily. In the active training process, the WDMs passively followed the active movement of lower limbs and exerted a desired resultant force on the shank. For each WDM, it was a force servo system, or rather a typical passive force servo system [16]. The motion of the lower limbs had great influence on the control accuracy of the passive force servo system. The major problem in researching the passive loading system lay in designing the forward force controller and the surplus force compensator.

2. Mechanical construction and dynamics modeling

2.1. Mechanical construction of the WDM

Figure 2 illustrates the composition of the WDM. The WDM consisted of a torque motor that drove a traction pulley directly. An increment encoder was located on the motor, and the encoder's readings were used to determine the wire elongation. The pose state and localization of the lower limbs could

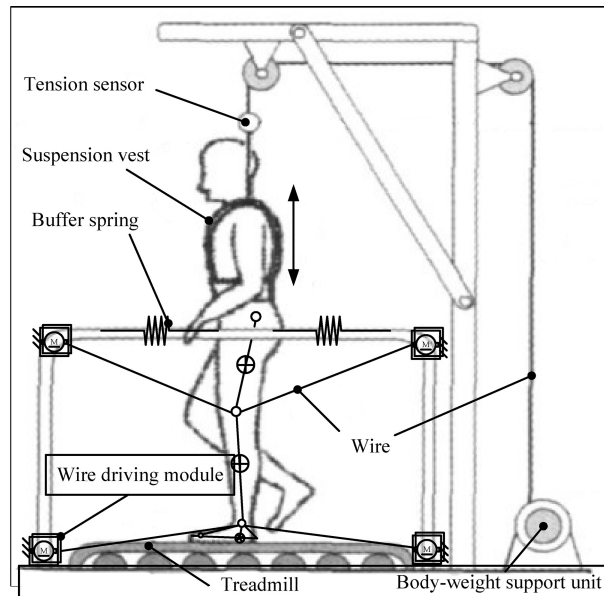
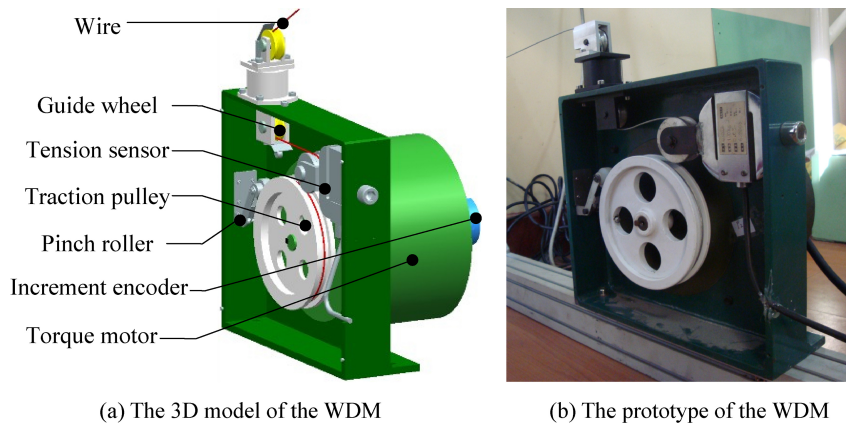


Fig. 1. Structural scheme of the wire driving lower limb rehabilitation robot.



(a) The 3D model of the WDM

(b) The prototype of the WDM

Fig. 2. Composition of the WDM.

be further determined. A pinch roller, fixed on the side frame, served to confine the wire to the traction pulley groove. A tension sensor was fixed on the other side of the frame, and a guide wheel was located on the opposite part of the tension sensor. After passing through the guide wheel, the wire's motion direction changed by 180° . The tension of the sensor was twice as much as the wire. Finally, the wire connected to the target after passing through a fixed guide wheel and a rotating guide wheel.

2.2. Wire driving dynamics model

On the basis of the mechanical construction, the mechanism model of the WDM is shown in Fig. 3. The WDM loaded the tension on the lower limbs through the wire. The wire was simplified into a mass-

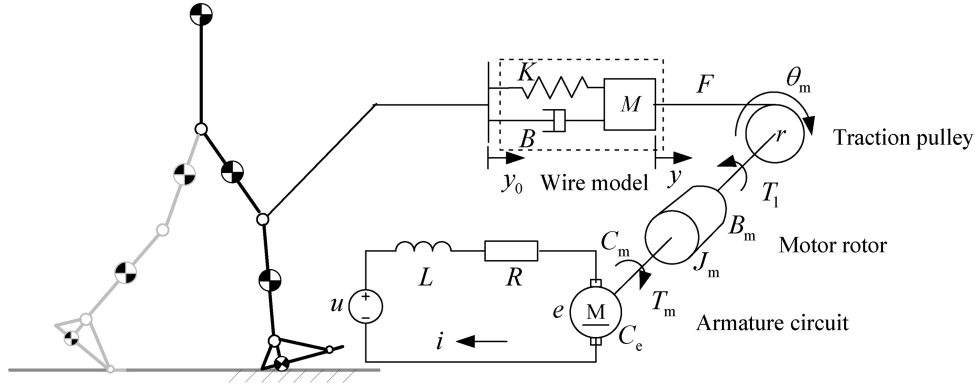


Fig. 3. Mechanism model of the WDM.

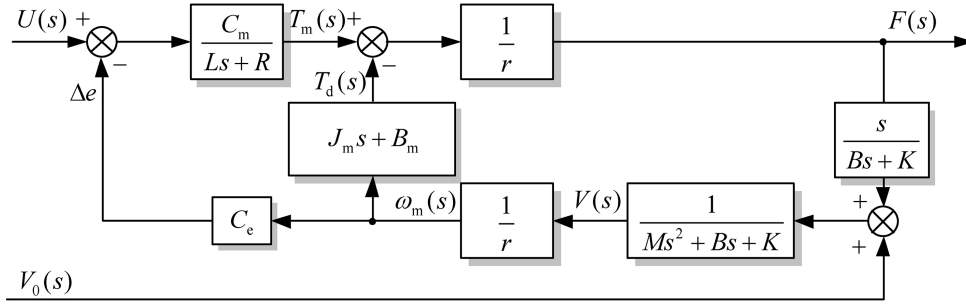


Fig. 4. Block diagram of the WDM.

spring-damping model for its low vibration frequency in the training process to clarify the effect of the wire more clearly.

The block diagram of the WDM is shown in Fig. 4. The output F was affected the motor armature voltage u and the disturbance v_0 caused by movements of the lower limbs.

Based on Fig. 4, the wire driving dynamics model of the WDM was as follows:

$$F(s) = M_1(s)U(s) - M_2(s)V_0(s) \quad (1)$$

where $V_0(s)$ is the velocity of the traction point, $V_0(s) = sY_0(s)$.

$M_1(s)$ is the transfer function from the motor armature voltage u to the tension F . It is the transfer function of the forward channel.

$$M_1(s) = \frac{C_m r (Ms^2 + Bs + K)}{J_e L s^3 + (B_e L + J_e R) s^2 + (B_e R + C_m C_e + K L r^2) s + K R r^2} \quad (2)$$

$M_2(s)$ is the transfer function from the input velocity disturbance v_0 to the output surplus force F . It is the transfer function of the disturbance channel.

$$M_2(s) = \frac{(Bs + K)[J_m L s^2 + (B_m L + J_m R) s + (B_m R + C_m C_e)]}{J_e L s^3 + (B_e L + J_e R) s^2 + (B_e R + C_m C_e + K L r^2) s + K R r^2} \quad (3)$$

In Eqs (2) and (3), $J_e = Mr^2 + J_m$ is the equivalent moment of inertia, and $B_e = Br^2 + B_m$ is the equivalent viscous friction coefficient.

The nominal value of each parameter in the WDM dynamics model is shown in Table 1.

Table 1
Parameters of the wire driving dynamics model

Parameter	Value	Parameter	Value
R/Ω	5	$J_m/(\text{kg}\cdot\text{m}^2)$	0.027
L/H	0.008	r/m	0.060
$C_e/[\text{V}\cdot(\text{rad/s})^{-1}]$	3.82	M/kg	0.036
$C_m/(\text{N}\cdot\text{m}\cdot\text{A}^{-1})$	3.15	$K/(\text{N}\cdot\text{m}^{-1})$	1×10^5
$B_m/(\text{N}\cdot\text{m}\cdot\text{s}\cdot\text{rad}^{-1})$	0.0106	$B/(\text{N}\cdot\text{s}\cdot\text{m}^{-1})$	30

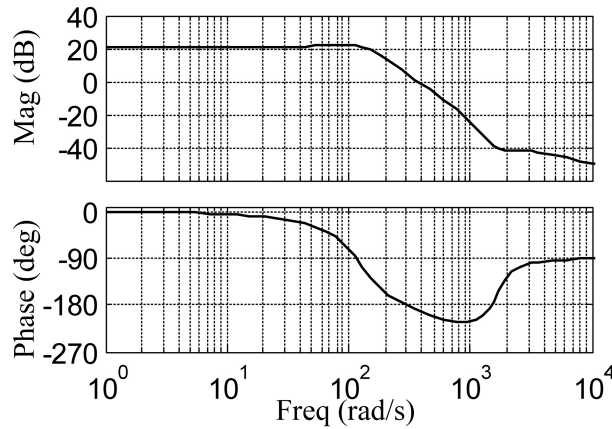


Fig. 5. Bode diagram of $M_1(s)$.

2.3. Characteristic analysis

The frequency characteristic of $M_1(s)$ is described in Fig. 5. In the working frequency (within 100 rad/s), the amplitude curve of $M_1(s)$ was approximately 20 dB; the phase curve was approximately a linear slant line. These characteristics provided some conveniences in the correction of the forward channel. In the low-frequency band, the amplitude curve of $M_1(s)$ did not need to be corrected. However, the phase response of $M_1(s)$ presented an overall phase lagging characteristic (approximately 1°) and a phase lag of 35° at 62.8 rad/s.

$M_1(s)$ was a type 0 system due to the lack of integral element in the denominator. The main control problem for $M_1(s)$ lay in increasing the system type to improve the static precision. However, the phase reserve would decrease and the stability of the system could not be guaranteed for the introduction of an integral element. To guarantee the stability, the open-loop gain needed to be reduced. But the response speed would slow down for the reduction of the open-loop gain. Therefore, the WDM forward controller needed to balance the static precision and response speed simultaneously.

The Bode diagram of $M_2(s)$ is shown in Fig. 6. The amplitude of the surplus force increased and the phase of the surplus force was slightly prior to the velocity disturbance $V_0(s)$ for the first-order differential element in $M_2(s)$ in the low-frequency band with the increase in the disturbance frequency. When the disturbance frequency was higher than 126 rad/s, the amplitude of the surplus force decreased with the increase in the velocity frequency for the second-order oscillation element in $M_2(s)$. The phase of the surplus force lagged behind the velocity disturbance ($< 90^\circ$).

The surplus force could not be completely eliminated due to the following reasons: (1) The surplus force caused by the motion of the lower limb affected the output directly. However, the compensation, generated by the controller, always lagged behind the output. (2) The change in the work environment

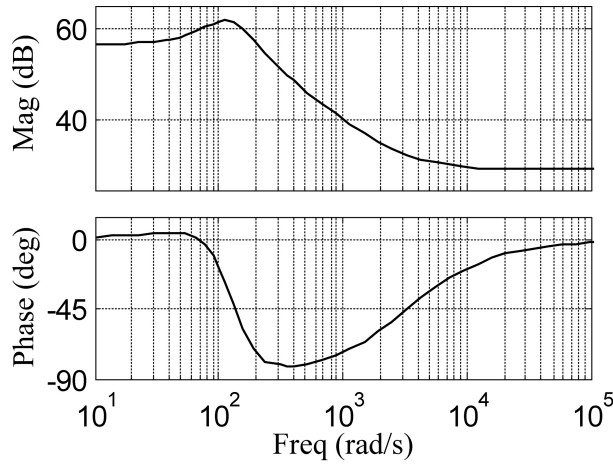


Fig. 6. Bode diagram of $M_2(s)$.

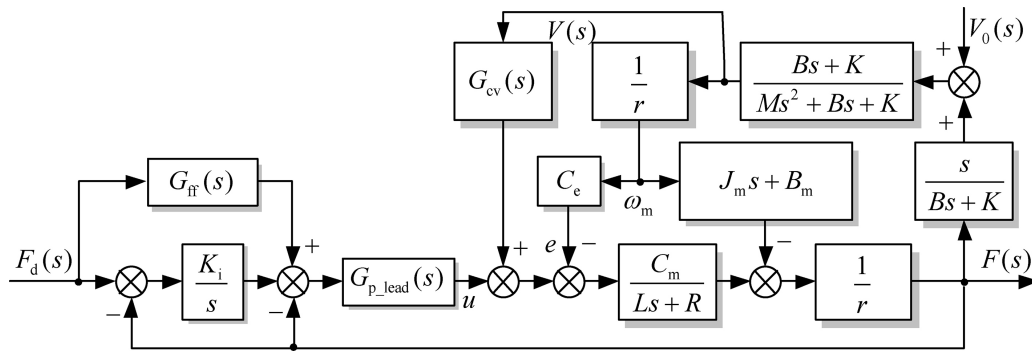


Fig. 7. Multiple feedback loop force control strategy for the wire driving system.

resulted in the variation in the dynamics model of WDM for the nonlinearity and time variation of the system, which made it difficult to design the surplus force compensator.

It is demanded that the surplus force reduction rate λ should exceed 90% to ensure the loading precision during the active training process. The experimental results confirmed that the remaining 10% surplus force was imperceptible to the subject.

$$\lambda = \frac{F_0 - F}{F_0} \times 100\% \tag{4}$$

In Eq. (4), F_0 is the surplus force before compensation and F is the surplus force after compensation. Normally, the motion frequency of the lower limbs would not exceed 3 Hz. This required that the surplus force reduction rate λ exceeded 90% when the disturbance frequency was within 3 Hz.

3. Control strategy

The multiple feedback loop force control strategy for the wire driving passive force servo system is shown in Fig. 7.

The control strategy design for the passive force servo system should consider two aspects: (a) A forward controller should be designed based on the forward channel transfer function $M_1(s)$ to improve the response speed and precision of the force control. (b) A surplus force compensator should be designed to minimize the negative impact of the velocity disturbance v_0 [17,18]. The forward controller consisted of an integral element, a local negative feedback element $G_{p_lead}(s)$, and a feed-forward element $G_{ff}(s)$. The surplus force compensator $G_{cv}(s)$ was designed based on the structure invariance principle.

An integral element was adopted as the primary control element for $M_1(s)$, which improved the system from 0-type to I-type. However, a single integral element would decrease the phase reserve and lower the dynamic quality.

In this case, a local negative feedback element $G_{p_lead}(s)$ (a second-order phase-lead element), composed of a proportional element K_a , a second-order oscillation element, and a second-order differentiation element, could be used to improve the system's dynamic quality.

$$G_{p_lead}(s) = K_a \frac{\frac{s^2}{\omega_{an}^2} + 2\xi_{an} \frac{s}{\omega_{an}} + 1}{\frac{s^2}{\omega_{ad}^2} + 2\xi_{ad} \frac{s}{\omega_{ad} + 1}} \quad (5)$$

Under the premise of ensuring stability, the feed-forward element $G_{ff}(s)$ in combination with the local negative feedback element $G_{p_lead}(s)$ could enhance the response speed of the system. Essentially $G_{ff}(s)$ was a proportional element. When the input $F_d(s)$ changed rapidly, the slow response of the primary controller for the integral element had a significant attenuation influence on input signals. Meanwhile, the input $F_d(s)$ transmitted to the phase-corrected system by dint of $G_{ff}(s)$. The force servo system worked in an open-loop state approximately, and the response speed of the system could be brought into play adequately. When the force servo system reached a stable state, the impact of the integral element was gradually seen. The steady-state accuracy was improved.

With reference to the block diagram of the WDM in Fig. 4 and Eq. (1), the surplus force was generated by the input velocity disturbance v_0 . Therefore, it was the most direct and effective method to compensate the surplus by using the traction point velocity v_0 . Furthermore, based on the structure invariance principle, the surplus force compensator was

$$G_{cv0}(s) = \frac{M_2(s)}{M_1(s)} = \frac{(Bs + K)[J_m L s^2 + (B_m L + J_m R)s + (B_m R + C_m C_e)]}{C_m r (M s^2 + Bs + K)} \quad (6)$$

Actually, the velocity of the traction point v_0 could not be measured precisely. Given that the stiffness of the wire was large enough, the velocity of the traction point v_0 and the velocity of the WDM v were approximately equal. Moreover, considering the physical realizability, a first-order low-pass filter was introduced into the surplus force compensator. The modified surplus force compensator was

$$G_{cv}(s) \approx G_{cv0}(s) = \frac{(Bs + K)[J_m L s^2 + (B_m L + J_m R)s + (B_m R + C_m C_e)]}{C_m r (M s^2 + Bs + K)(\tau s + 1)} \quad (7)$$

4. Experimental evaluation

Passive loading experiment was performed in this section to further confirm the effectiveness of the multiple feedback loop force controller. The experimental platform is shown in Fig. 8. The bearing unit was a position servo system. The loading unit, following the bearing unit passively and exerting a force on the bearing unit, was a force servo system.

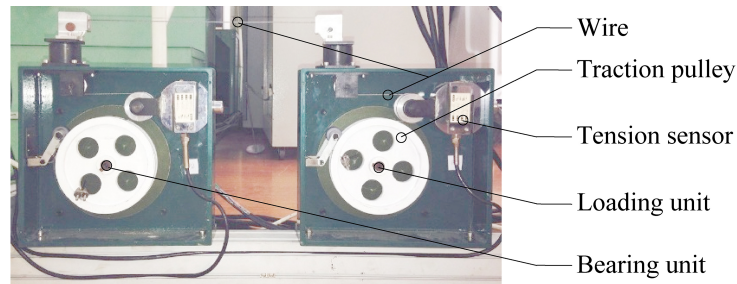


Fig. 8. Experimental platform of the multiple feedback loop control for passive loading.

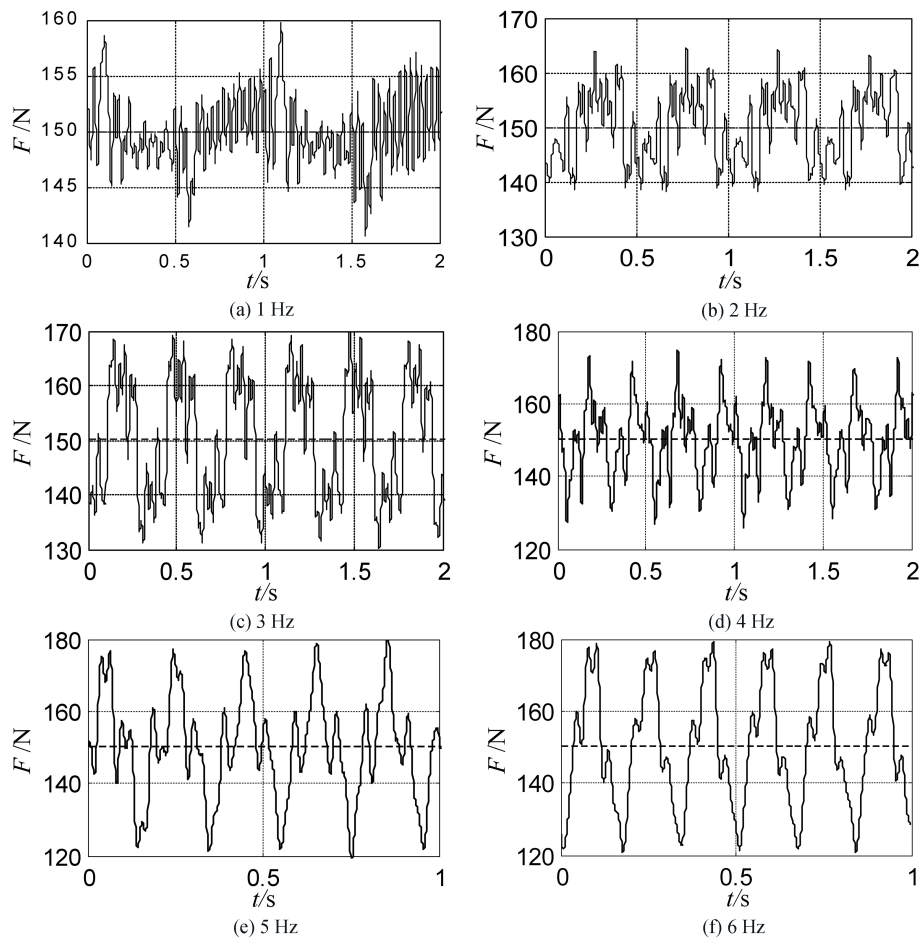


Fig. 9. Surplus force of the wire driving module with different frequency velocity disturbance input.

With reference to the multiple feedback loop force control strategy in Fig. 7, the wire tension F and the velocity of the bearing unit v were used as the feedback signals. The desired force F_d of the passive loading was 150 N. The velocity amplitude of the bearing unit v (sine wave) was 0.3 m/s. The results of passive loading when the velocity frequency changed from 1 to 6 Hz are shown in Fig. 9, and the statistical results of the surplus force reduction rate are described in Table 2.

Table 2
Statistical results of the multiple feedback loop control for passive loading

Velocity frequency, Hz	1	2	3	4	5	6
Velocity amplitude, m·s ⁻¹	0.3					
Surplus force before compensation, N	202.14	204.24	207.54	212.64	218.58	226.01
Surplus force after compensation, N	10	14	19	23	28	29
Surplus force reduction rate, λ (%)	95.05	93.15	90.85	89.18	87.19	87.17

The theoretical surplus force compensator was simplified based on the dominant pole placement to facilitate implementation of the experiments. The experiments results indicated that the multiple feedback loop force controller could decrease the surplus force efficiently and improve the precision. The designed controller could meet the performance requirements of lower limb rehabilitation.

5. Conclusions and future work

This study presented the mechanical design of the WDM and experimental evaluation of a wire driving lower limb rehabilitation robot. The dynamics model of the WDM was provided, based on which a forward controller and a surplus force compensator for WDM were designed. The experiments demonstrated that the WDM could load force accurately and reliably during the loading procedure. The machinery and control system of the WDM achieved the design request.

Future work will focus on control methodologies for the robot to improve the force control accuracy. Further experimental and clinical studies will be conducted to determine the efficacy and safe applicability of the robot in human subjects.

Acknowledgments

This project is supported by National Natural Science Foundation of China (Grant No. 51705534), Fundamental Research Funds for the Central Universities No. 18CX02085A and Shandong Provincial Natural Science Foundation No. ZR2016EEB12.

Conflict of interest

None to report.

References

- [1] Meng W, Liu Q, Zhou Z, et al. Recent development of mechanisms and control strategies for robot-assisted lower limb rehabilitation. *Mechatronics*, 2015; 31: 132-145.
- [2] Kumru H, Murillo N, Benito-Penalva J, et al. Transcranial direct current stimulation is not effective in the motor strength and gait recovery following motor incomplete spinal cord injury during Lokomat[®] gait training. *Neuroscience letters*, 2016; 620: 143-147.
- [3] Wall A, Borg J, Palmcrantz S. Clinical application of the Hybrid Assistive Limb (HAL) for gait training – a systematic review. *Frontiers in systems neuroscience*, 2015; 9.
- [4] Esquenazi A, Talaty M, Packel A, et al., The ReWalk powered exoskeleton to restore ambulatory function to individuals with thoracic-level motor-complete spinal cord injury. *American Journal of Physical Medicine & Rehabilitation*, 2012; 91(11): 911-921.

- [5] Hesse S, Waldner A, Tomelleri C. Innovative gait robot for the repetitive practice of floor walking and stair climbing up and down in stroke patients. *Journal of NeuroEngineering and Rehabilitation*, 2010; 7: 30-40.
- [6] Winstein CJ, Wolf SL, Dromerick AW, et al. Effect of a task-oriented rehabilitation program on upper extremity recovery following motor stroke: the ICARE randomized clinical trial. *Jama*, 2016; 315(6): 571-581.
- [7] Pott A, Bruckmann T. *Cable-Driven Parallel Robots*. Springer Berlin Heidelberg, 2013.
- [8] Trevisani A. Planning of dynamically feasible trajectories for translational, planar, and underconstrained cable-driven robots. *Journal of Systems Science and Complexity*, 2013; 26(5): 695-717.
- [9] Mao Y, Jin X, Dutta GG, et al. Human movement training with a cable driven arm exoskeleton (carex). *IEEE Transactions on Neural Systems and Rehabilitation Engineering*, 2015; 23(1): 84-92.
- [10] Jin X, Cui X, Agrawal SK. Design of a cable-driven active leg exoskeleton (c-alex) and gait training experiments with human subjects. *2015 IEEE International Conference on Robotics and Automation (ICRA)*. 2015; 5578-5583.
- [11] Alamdari A, Krovi V. Design and analysis of a cable-driven articulated rehabilitation system for gait training. *Journal of Mechanisms and Robotics*, 2016; 8(5): 051018.
- [12] Alamdari A, Krovi V. Parallel articulated-cable exercise robot (PACER): novel home-based cable-driven parallel platform robot for upper limb neuro-rehabilitation. *Proceedings of the ASME 2015 International Design Engineering Technical Conferences and Computers in Engineering Conference*, August. 2015; 2-5.
- [13] Surdilovic D, Zhang J, Bernhardt R. STRING-MAN: Wire-robot technology for safe, flexible and human-friendly gait rehabilitation. *IEEE 10th International Conference on Rehabilitation Robotics*. 2007; 446-453.
- [14] Wang KY, Di CB, Tang XQ, et al. Modeling and Simulation to Muscle Strength Training of Lower Limbs Rehabilitation Robots. *Advances in Mechanical Engineering*, 2014.
- [15] Rosati G, Masiero S, Rossi A. On the Use of Cable-Driven Robots in Early Inpatient Stroke Rehabilitation. *Advances in Italian Mechanism Science*. Springer International Publishing, 2017; 551-558.
- [16] Hirata Y, Shirai R, Kosuge K. Position and orientation control of passive wire-driven motion support system using servo brakes. *2017 IEEE International Conference on Robotics and Automation (ICRA)*. 2017; 3702-3707.
- [17] Lin X, Zhang R. H (A) Control for Stochastic Systems with Poisson Jumps. *Journal of Systems Science & Complexity*, 2011; 24(4): 683-700.
- [18] Li Y, Zhang W, Liu X. Stability of Nonlinear Stochastic Discrete-Time Systems. *Journal of Applied Mathematics*, 2013.